The glass transition and enthalpy recovery of polystyrene nanorods using Flash differential scanning calorimetry \odot

Special Collection: Polymer Nanoconfinement

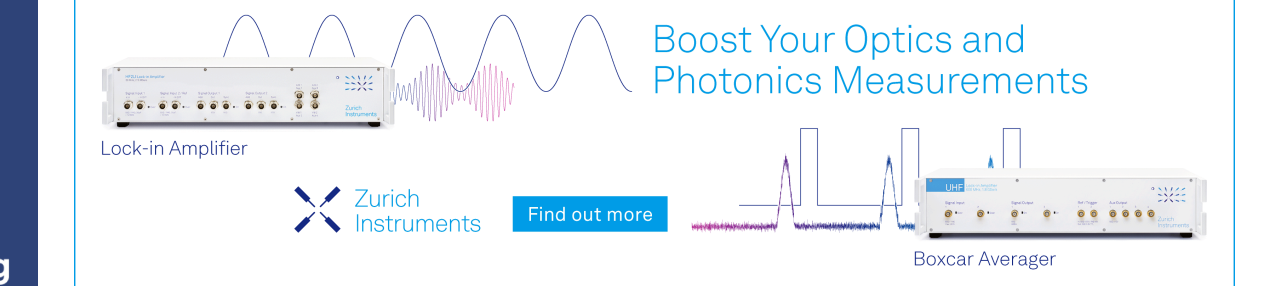
Madhusudhan R. Pallaka [®] ; Sindee L. Simon ■ [®]



J. Chem. Phys. 160, 124904 (2024) https://doi.org/10.1063/5.0190076









10 April 2024 13:42:08

The glass transition and enthalpy recovery of polystyrene nanorods using Flash differential scanning calorimetry

Cite as: J. Chem. Phys. 160, 124904 (2024); doi: 10.1063/5.0190076 Submitted: 3 December 2023 • Accepted: 31 January 2024 • Published Online: 27 March 2024







Madhusudhan R. Pallaka^{1,a)} D and Sindee L. Simon^{2,b)}





AFFILIATIONS

- Department of Chemical Engineering, Texas Tech University, Lubbock, Texas 79409, USA
- ²Department of Chemical and Biomolecular Engineering, North Carolina State University, Raleigh, North Carolina 27695, USA

Note: This paper is part of the JCP Special Topic on Polymer Nanoconfinement.

- ^{a)}E-mail: madhusudhan.pallaka@intel.com
- b) Author to whom correspondence should be addressed: slsimon@ncsu.edu

ABSTRACT

The glass transition (Tg) behavior and enthalpy recovery of polystyrene nanorods within an anodic aluminum oxide (AAO) template (supported nanorods) and after removal from AAO (unsupported nanorods) is studied using Flash differential scanning calorimetry. Tg is found to be depressed relative to the bulk by 20 ± 2 K for 20 nm-diameter unsupported polystyrene (PS) nanorods at the slowest cooling rate and by 9 ± 1 K for 55 nm-diameter rods. On the other hand, bulk-like behavior is observed in the case of unsupported 350 nm-diameter nanorods and for all supported rods in AAO. The size-dependent Tg behavior of the PS unsupported nanorods compares well with results for ultrathin films when scaled using the volume/surface ratio. Enthalpy recovery was also studied for the 20 and 350 nm unsupported nanorods with evolution toward equilibrium found to be linear with logarithmic time. The rate of enthalpy recovery for the 350 nm rods was similar to that for the bulk, whereas the rate of recovery was enhanced for the 20 nm rods for down-jump sizes larger than 17 K. A relaxation map summarizes the behavior of the nanorods relative to the bulk and relative to that for the 20 nm-thick ultrathin film. Interestingly, the fragility of the 20 nm-diameter nanorod and the 20 nm ultrathin film are identical within the error of measurements, and when plotted vs departure from T_g (i.e., $T - T_g$), the relaxation maps of the two samples are identical in spite of the fact that the T_g is depressed 8 K more in the nanorod sample.

Published under an exclusive license by AIP Publishing. https://doi.org/10.1063/5.0190076

INTRODUCTION

Properties of polymers under nanoconfinement have been of significant interest due to their role in many practical applications, including coatings, composites, and membranes, and nano- and microelectronics. Among the key properties, the glass transition temperature (Tg) has been well studied and is found to be significantly affected at the nanoscale when compared with that at the bulk. At the nanoscale, Tg can increase, decrease, or remain unchanged depending on the nanoconfinement geometry, interaction between the confined material and any substrate present, and molecular structure and architecture of the glass former.^{3–8} The influence of nanoconfinement geometry on T_g is of particular interest because it may allow unraveling of surface vs intrinsic confinement effects given the different surface to volume ratios of different geometries.

In the case of polystyrene (PS), the size-dependent T_g of 1D ultrathin films has been extensively studied using various experimental techniques for supported, freestanding, sandwiched, and stacked films. $^{1,5,9-32}$ In general, for polystyrene, $T_{\rm g}$ is depressed in ultrathin films on neutral or weakly interacting substrates, and a nonlinear dependence on film thickness (h), independent of molecular weight is reported:9

$$T_g(h) = T_g^{bulk} \left[1 - \left(\frac{\alpha}{h} \right)^{\delta} \right], \tag{1}$$

where $T_g(h)$ is the glass transition temperature at film thickness h, T_g^{bulk} is the bulk glass transition temperature (373.8 \pm 0.7 K for polystyrene), and α and δ are the fitting parameters whose

values have been reported to be 1.3 nm and 1.28, respectively. 10 The existence of a $T_{\rm g}$ depression for ultrathin films has been generally attributed to an interplay of enhanced mobility at the free surface, the influence of the substrate, and intrinsic size effects. $^{1,2,5,9-38}$

Work on the size-dependent Tg of 2D polystyrene nanorods is considerably more sparse and has been mainly carried out using anodic aluminum oxide (AAO) nanopores³⁹⁻⁴² as a support or for nanorods in aqueous dispersion. Zhu and co-workers reported a 3 K increase in T_g for polystyrene (M_w = 280 kg/mol) inside AAO nanopores irrespective of pore diameter; they also reported a depression of 24 K for aqueous dispersed 100 nm-diameter PS wires prepared via electrospinning.³⁹ On the other hand, Torkelson and co-workers⁴⁰ reported a T_g depression for polystyrene supported nanorods when $d \le 2R_g$ where d is the diameter of nanorods and R_g is the radius of gyration—and a depression of 8 K was reported for 24 nm polystyrene rods with a molecular weight (M_w) of 1420 kg/mol. On the other hand, Floudas and co-workers similarly observed a 4 K depression in 25 nm-diameter AAO, but for polystyrene trimer, $^{\! 41}$ which is molecularly much smaller than the pore size; the result was attributed to interfacial interactions. Moreover, Xue and co-workers⁴² also studied low molecular weight (6-60 kg/mol) PS in AAO pores as small as 25 nm and reported bulk values at the highest rates (120 K/s) but observed 2 Tgs at intermediate cooling rates (10 K/min), which were attributed to thermal stresses.

In the case of 3D-confined polystyrene nanospheres, the size-dependent glass transition behavior has been studied by Priestley and co-workers, 43,44 who reported T_g depressions for aqueous dispersed and air exposed nanospheres for sphere diameters (d) less than 400 nm, with a 56 K depression observed for d = 90 nm. When the nanospheres were capped with silica, 43 no T_g depressions were observed. Cangialosi and co-workers laso reported T_g depressions of similar order of magnitude for PS nanospheres on poly(dimethylsiloxane) by Flash differential scanning calorimetry (DSC), with a depression of 24 K observed for d = 230 nm.

The glass transition temperature is a kinetic phenomenon and depends on the cooling rate,4 and it is well known that the changes in Tg of nanoconfined polymers also depend on the cooling rate. 1,2,13,34,45 A process intimately related to Tg is that of structural recovery, which is the slow evolution of a glass toward its equilibrium volume or enthalpy by segmental relaxation.4 In our own laboratory, extensive studies have been performed using both conventional and Flash differential scanning calorimetry on the enthalpy recovery of stacked²¹ and ultrathin PS films, ^{46–50} as well as bulk PS.51,52 In the case of stacked PS films aged over a narrow range of temperatures up to 15 K below Tg, the overall rate of enthalpy recovery was reported to be accelerated relative to the bulk at a given aging temperature, but similar when compared at aging temperatures at the same distance from their nominal (or reference) Tg values.1 In the case of ultrathin PS films, enthalpy recovery of single 20 nm ultrathin film was studied on the Flash DSC; the overall rate of enthalpy recovery in the glassy state for a single 20 nm-thick ultrathin polystyrene film was found to be faster when compared with 1.1 μ m thick film (bulk) at aging temperatures between 20 and 70 K below Tg. ^{2,47,48} Boucher and co-workers also reported enhanced enthalpy recovery in the case of stacked PS films when compared with the bulk, but these comparisons were made at same aging temperatures rather than at same jump size from T_g. ⁵³ On the other hand, reduced structural recovery rates were reported by Pye and Roth for volume recovery studies on 30 nm ultrathin PS film over a broad temperature range⁵⁴ and by Frieberg, Glynos, and Green for experiments performed as a function of aging temperature on linear and star-shaped PS thin films.⁵⁵

The influence of spatial dimensionality and geometry of nanoconfinement on the structural recovery of polystyrene has also been examined. Zhu and co-workers studied enthalpy recovery of aqueous dispersed and AAO supported PS nanowires, where the rate of enthalpy recovery below Tg was found to be reduced in both systems when compared with the bulk.³⁹ Priestley, Fytas, and co-workers investigated the enthalpy relaxation of aqueous dispersed and silica-capped 3D PS nanospheres, and they found accelerated enthalpy recovery rates in the case of aqueous dispersed PS nanospheres and reduced rates in the case of silica-capped PS nanospheres.⁵⁶ Cangialosi and co-workers also reported enhanced enthalpy recovery rates in the case of PS nanospheres on poly(dimethyl siloxane).⁴⁵

In this work, we examine the Tg and enthalpy recovery of polystyrene nanorods, both unsupported rods and those supported in anodic aluminum oxide (AAO) templates. We choose to study high molecular polystyrene in order that the chains from adjacent nanorods do not have any significant diffusion across the nanorod boundary in the time scale of the experiments. We exploit Flash differential scanning calorimetry to make the measurements, which has advantages including the ability to use nanogram samples, sensitivity to aging times as short as 0.01 s, and ability to access aging temperatures of T_g + 15 °C for the high fictivetemperature glass created by cooling at very high rates (1000 K/s). The feasibility of the use of AAO templated nanopores as a form of nanoconfinement on the Flash DSC has been previously demonstrated in our group where size-dependent melting behavior of n-alkanes was successfully studied.⁵⁷ The T_g and structural recovery results will be compared with results from the literature for other nanoconfinement geometries in order to ascertain the importance of surface in dictating the observed behavior.

EXPERIMENTAL

Materials

The high-molecular-weight atactic polystyrene (PS) used in this study is from Polymer Source Inc. The weight-average molecular weight (M_w) and the number-average molecular weight (M_n) of the as-received PS is 2000 ± 110 kg/mol and 1700 ± 150 kg/mol based on our own measurements using gel permeation chromatography (Tosoh EcoSEC) with an RI detector; the manufacturer reported 2400 and 2100 kg/mol, respectively. After infiltration of the material into the AAO templates (as described in the next section), the molecular weight decreases with $M_w = 1000 \pm 180$ kg/mol and $M_n = 675 \pm 80$ kg/mol. However, due to the high molecular weights involved, this change in molecular weight is anticipated to result in an insignificant change in Tg, i.e., less than 0.1 K.⁵⁸

AAO templates having pore diameters of 55 ± 2 nm (from Synkera Technologies, USA) and pores sizes of 20 ± 2 nm and 350 ± 45 nm (from Universidad de Oviedo, Spain) were used to synthesize PS nanorods. These templates are the same as those used to study melting of nanoconfined alkanes by Flash DSC in

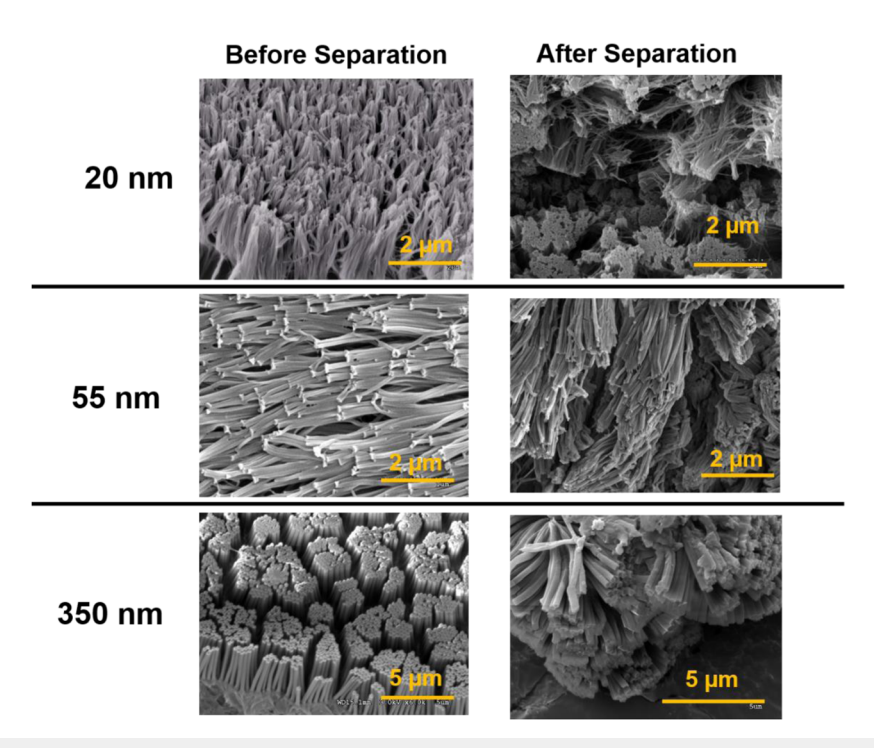


FIG. 1. Scanning electron micrographs of unsupported polystyrene nanorods after dissolving the AAO template and before (on left) and after (on right) separation from the excess PS film substrate. The samples were sputtered with a thin layer of iridium (2–5 nm) before imaging.

previous work, ⁵⁷ and the thickness of the AAO templates is 5 μ m in order to minimize thermal lag effects in the Flash DSC. ^{59–61} Prior to the synthesis of our nanorods, the AAO templates were rinsed with methanol several times and then dried for 2 h *in vacuo* at 150 °C; prior to use, templates were stored in a desiccator to minimize absorption of adventitious moisture.

Polystyrene nanorods were synthesized by vacuum melt infiltration of a precursor polystyrene film into an AAO template.⁶², In the case of supported polystyrene nanorods (i.e., those that will be studied in the AAO template), the thickness of the precursor film was chosen to exactly fill the pores of the AAO template. After various trials based on the available volume in the pores, PS films with thicknesses of 0.45, 0.70, and 1.3 μ m were used for infiltration into 20, 55, and 350 nm-diameter AAO templates, respectively. The precursor films were produced by spin-coating concentrated (~10 wt.%) polystyrene/toluene solutions (using HPLC-grade, 99.99% pure toluene) onto cleaved mica; subsequently, the films were floated on water, picked up by a tweezer, and dried for 48 h under vacuum at 50 °C before they were placed atop the AAO template for infiltration. The vacuum infiltration process was performed at 190 °C for 4 h to yield AAO supported PS nanorods of a given diameter.

In the case of unsupported PS nanorods, a thicker polystyrene film (\sim 50 μ m), prepared by compression molding under vacuum in a hot press at 170 °C, was chosen to infiltrate into the AAO templates using the same conditions as for the supported PS nanorods. After infiltration, the AAO template was removed by dissolving it in 1 M sodium hydroxide solution; the supernatant and the excess

PS film holding the PS nanorods were vacuum filtered using excess deionized (DI) water and then dried *in vacuo* at 50 °C for 24 h. For the Flash DSC sample, the PS nanorods are separated from the excess PS film by delicately cutting them with a scalpel. SEM images of unsupported PS nanorods are shown in Fig. 1. Images were captured using a Hitachi S-4300 high resolution SEM after removal of the AAO template and both before and after the separation of nanorods from the excess PS film substrate.

Flash differential scanning calorimetry

The glass transition behavior and enthalpy recovery of the polystyrene nanorods were studied using a Mettler Toledo Flash DSC 1 with a Freon intercooler and 20 ml/min nitrogen gas purge. Prior to the measurements, a temperature calibration was performed using phenanthrene ($T_{\rm m}=98.7\,^{\circ}\text{C}$) on the reference side of the chip. In addition, a correction factor for the thermal gradient in the films during heating scans at 600 K/s is applied to the $T_{\rm g}$ data and is equal to the average of the difference between glass transition temperatures measured on cooling and subsequent heating at \pm 600 K/s following the recommendation of Schawe, 61 this correction was in the range of 3–4 K for unsupported PS nanorods and 6–9 K in the case of AAO supported PS nanorods.

In the case of AAO supported nanorods, a small piece (<0.09 mm²) was cut from the parent template containing polystyrene nanorods and transferred onto the center of the chip sensor with the help of a hair. For unsupported PS nanorods, the rods were first separated from the excess PS film substrate using

a micro-scalpel and then these nanorods were transferred using a hair to the center of the Flash DSC chip sensor. A small amount of [C₇C₁im] [NTf₂] ionic liquid was added for better thermal contact; no plasticization was observed, but a slight increase (~2 K) in T_g was observed when compared with bare nanorods due to improved

For measurement of T_{g} as a function of cooling rate, a given sample was heated to 180 °C at 600 K/s after cooling from 180 to 30 °C at rates ranging from 0.1 to 1000 K/s. Heating scans for a given cooling rate were repeated ten times and were averaged to improve the signal-to-noise ratio. The runs made after cooling at 600 K/s were also examined prior to averaging in order to verify that data were reproducible and that there was no drift in the data.

In addition to the Tg studies, enthalpy recovery experiments were also performed on the 20 nm and 350 nm-diameter unsupported nanorods. Samples were aged isothermally after cooling at 1000 K/s from 190 °C at various isothermal aging temperatures for aging times (t_a) ranging from 0.01 to 86 400 s (24 h) at each temperature. Each isothermal aging step was followed by cooling to 30 °C, heating of the aged material to 190 °C, cooling to 30 °C, and then heating of the unaged material to 190 °C. The heating scan of the aged material is followed immediately by an unaged reference scan in order to serve as an internal standard; in addition, this unaged reference scan remains unchanged during the course of the enthalpy recovery experiments, indicating that no mass loss or degradation

We characterize the structure of our glass formed after cooling at different rates or after isothermal aging by the fictive temperature, T_f,⁶⁴ which is defined as the temperature where the extrapolated glass line from the state of interest intersects the liquid line. Thus, by definition, if the material is at equilibrium (i.e., on the liquid line), then $T_f = T$. On the other hand, after cooling at a given cooling rate q to the glassy state, if no isothermal aging has occurred, T_f is called the limiting fictive temperature, T_f', and it is equivalent to the T_g value (within 1-2 K) that would be measured on cooling at that same cooling rate q_i^{65} for this reason, $T_f{}'$ is interchangeably referred to as Tg in the text. In the case of isothermal aging at aging temperature T_a , T_f will decrease from its initial value of $T_{fo} = T_g(q)$ to its equilibrium value on the liquid line, where T_f is expected to reach T_a . The fictive temperature is determined from the Flash DSC heat flow data using Moynihan's method [Eq. (2)]66 or Richardson's method $[Eq. (3)]:^6$

$$\int_{T_f'}^{T\gg T_g} (\dot{Q}_l - \dot{Q}_g) dT = \int_{T\ll T_g}^{T\gg T_g} (\dot{Q} - \dot{Q}_g) dT, \tag{2}$$

$$\int_{T_f'}^{T\gg T_g} (\dot{Q}_l - \dot{Q}) dT = 0, \tag{3}$$

where \dot{Q}_l and \dot{Q}_g are the heat flows in the liquid and glassy states, respectively, and \dot{Q} is the apparent heat flow of the sample. The simplified Richardson's method is applicable to and was used only for aging scans whose onsets of devitrification are greater than T_f. Although for large enthalpy overshoots, the two equations are equivalent, we use Richardson's method because it does not require extrapolating the glass lines and hence it provides a more accurate and robust determination of T_f. The glass and liquid state heat flows in Eq. (2) and the liquid heat flows in Eq. (3) are obtained from

linear fits in these regimes after superposing all heat flow scans in order to ensure consistency in the determination of T_f.

The sample mass of the unsupported PS nanorods was obtained by symmetry analysis, 57,68 which involves correcting the measured heat flow of rods for heat losses and the addenda heat capacity of the empty chip, and then dividing the symmetry-corrected heat flow with glassy absolute heat capacity of polystyrene at a defined temperature. The sample masses of the 20, 55, and 350 nm-diameter unsupported polystyrene nanorods are 145, 86, and 350 ng, respectively. On the other hand, the sample mass of the polystyrene in the AAO supported rods was obtained by dividing the step change in heat flow observed at Tg by the step change in heat capacity for a bulk polystyrene; the sample masses are 74, 96, and 111 ng, respectively, for supported rods in 20, 55, and 350 nm AAO templates. We note that the sample will ideally cover the $0.3 \times 0.3 \text{ mm}^2$ area of the chip and be less than a few microns thick, but the actual mass that is picked up by the practitioner using a hair is variable and independent of the rod size (leading to the variability of the sample mass). Furthermore, the supported rod samples contain both the polystyrene rods and the AAO template and, thus, typically have a lower mass of polystyrene than the unsupported samples.

RESULTS

Tq of polystyrene nanorods

The change in $T_{\rm g}$ from the bulk for supported nanorods in AAO templates is shown in Fig. 2 vs rod diameter (d) for a cooling rate of 0.1 K/s, along with data from the literature. For our AAO supported nanorods, Tg is found to be independent of rod size and approximately 2-3 K higher than the bulk value at all cooling rates (shown later). The inset in Fig. 2 shows heating scans for the 20 nm rods in AAO after cooling at 1000 K/s and at 0.1 K/s; for the fastest cooling rates, there is clearly only one step change at Tg, and

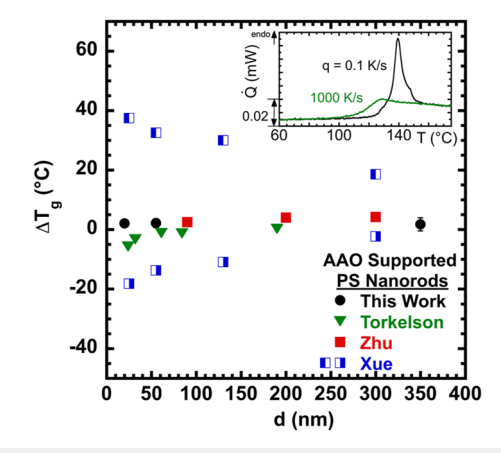


FIG. 2. Magnitude of $T_{\rm g}$ depressions for supported polystyrene nanorods in AAO nanoporous templates having pore diameter d, from this work (black filled circles) and the work of Torkelson and co-workers⁴⁰ (green inverted filled triangles); Zhu and co-workers³⁹ (red filled squares); and Xue and co-workers⁴² (ΔT_{q,hi} and $\Delta T_{q,lo}$: blue half-filled squares). The inset shows the heating scans for the 20 nm supported rods after cooling at rate q = 0.1 and 1000 K/s; curves are rotated for ease of viewing.

as the cooling rate decreases, the enthalpy overshoot increases and moves to higher temperatures, as expected, resulting in a decrease in limiting fictive temperature. There is no indication of two distinct Tg transitions although there is a small high temperature shoulder that appears in the largest enthalpy overshoots (e.g., for the 0.1 and 0.3 K/s cooling rates); this is not attributable to a second T_g , and although its origin is not fully understood, such high temperature shoulders in enthalpy recovery peaks at Tg are often present in nanocalorimetric heating scans of stable, aged, and slowly cooled glasses, even for bulk materials. 1,2,45,50,69,70 The T_g data in Fig. 2 are compared with results from the literature for supported nanorods. Our results are in good agreement with those reported by Zhu and co-workers³⁹ at a cooling rate of 10 K/min (0.17 K/s). The near absence of a T_g change has also been reported for other geometries where no free surface is present. 12,43 On the other hand, the results from Torkelson and co-workers⁴⁰ at a cooling rate of 40 K/min (0.67 K/s) and M_w = 1260 kg/mol show similar results to ours except below 50 nm, where a ~8 K Tg depression is reported for 24 nm-diameter rods. Xue and co-workers⁴² show two very distinct Tg transitions, one depressed and one elevated, for AAO supported PS nanorods of low molecular weight ($M_w = 6 \text{ kg/mol}$) at cooling rates of 10 K/min; their results contrast with our results and the others shown, perhaps due to low molecular weight used in their study, although Floudas and co-workers⁴¹ reported only a single T_g with a 4 K depression for polystyrene trimer in AAO.

We also examine the behavior of the polystyrene nanorods after removal of the AAO template. Representative Flash DSC heating scans are shown after cooling at various rates in Fig. 3 for the unsupported rods. As expected, the enthalpy overshoots grow and shift to higher temperatures as the cooling rate decreases, resulting in a decrease in limiting fictive temperature, as indicated by the arrows. Interestingly, both the step change in T_g and the overshoot occur at lower temperatures as the rod size decreases, clearly indicating a reduction in the glass transition temperature. A similar but smaller shift in the overshoot at T_g was also observed in the case of stacked thin films, 20 but for 20 nm ultrathin films 2 only a slight broadening

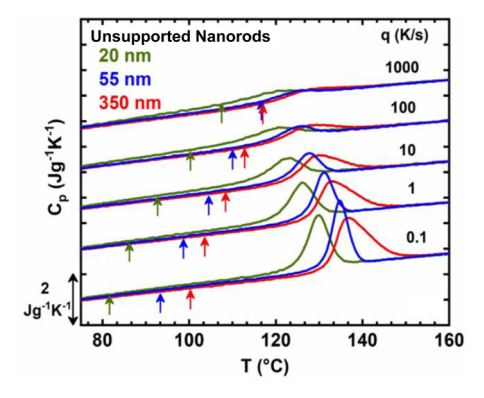


FIG. 3. Heat flow in heat capacity units vs temperature for unsupported polystyrene nanorods (after AAO removal) on heating at 1000 K/s after cooling at rates q of 1000, 100, 10, 1, and 0.1 K/s for rods of 20 (green), 55 (blue), and 350 (red) nm diameter. Arrows indicate the location of T_g as obtained from the Moynihan method for the fictive temperature.

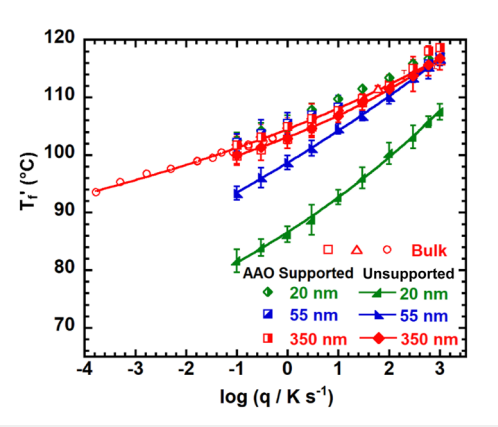


FIG. 4. The limiting fictive temperature as function of cooling rate for unsupported polystyrene nanorods and AAO supported nanorods; the data are compared with bulk films from previous work. ^{1,21} The solid lines are the WLF fits obtained from the parameters listed in Table I.

of the overshoot was observed on the low temperature side (rather than the shift to lower temperatures observed here).

The Tg reductions as a function of cooling rate are summarized in Fig. 4 where the glass transition temperature is plotted for all of our nanorod data, as well as for bulk polystyrene data from our previous studies. 1,21 As already mentioned, the supported rods in AAO show a 2-3 K elevation in T_g over bulk for all cooling rates, whereas the 350 nm unsupported PS rods show bulk-like behavior with the T_gs comparable to bulk polystyrene within the error of measurements. On the other hand, T_g depressions are observed for both 20 and 55 nm unsupported nanorods, with the magnitude of the depression decreasing with increasing cooling rate. For the 55 nm-diameter rods, ΔT_g <2 K at 1000 K/s and 8.8 \pm 0.7 K at 0.1 K/s. For the 20 nm-diameter rods, ΔT_g = 9.4 \pm 1.6 K at 1000 K/s and of 20.1 \pm 2.2 K at 0.1 K/s. The latter's T_g depression at 1000 K/s is in contrast to our previous studies on ultrathin polystyrene films on the Flash DSC, which showed no changes at this high cooling rate, 1,2 but several other materials have shown T_g depressions at cooling rates greater than 300 K/s, including ultrathin polycarbonate films³⁴ and polystyrene nanospheres.⁴³

The cooling rate-dependent T_g values shown in Fig. 4 are well described by the Williams–Landel–Ferry (WLF) equation:⁷¹

$$\log(q/q_0) = \frac{C_1(T_g - T_{g0})}{C_2 + (T_g - T_{g0})},\tag{4}$$

where q is the cooling rate, q_0 is the reference cooling rate where $T_g = T_{g0}$, which is chosen to be the value at 0.1 K/s, and C_1 and C_2 are the WLF parameters. The fitting parameters along with the normalized apparent activation energy for glass formation E_a/R and the dynamic fragility m are also shown in Table I, where these parameters are defined as

$$E_a/R = \frac{-d\ln q}{d(\frac{1}{T_g})} = 2.3C_1 T_{go}^2/C_2,$$
 (5)

$$m = \frac{-d\log q}{d(\frac{T_{g0}}{T_g})} = C_1 T_{go}/C_2.$$
 (6)

TABLE I. WLF parameters, normalized apparent activation energy E_a/R , and fragility m.

Sample	Diameter or thickness (nm)	T _{go} (K) ^a	C_1	C ₂ (K)	E _a /R (kK)	m
Unsupported nanorods	350	373.2 ± 1.6	12.1 ± 0.6	34.4 ± 2.4	113 ± 9	131 ± 11
	55	365.6 ± 1.2	22.0 ± 3.4	110.7 ± 17.2	62 ± 8	73 ± 7
	20	354.5 ± 2.0	13.6 ± 2.1	63.5 ± 5.0	62 ± 4	76 ± 13
AAO supported rods	350	374.9 ± 1.5	13.80 ± 0.9	40.2 ± 3.3	112 ± 8	129 ± 9
	55	375.3 ± 1.5	17.8 ± 4.6	50.5 ± 8.7	115 ± 9	134 ± 14
	20	375.2 ± 1.3	16.8 ± 3.2	50.1 ± 6.9	109 ± 9	126 ± 11
Thin films ^b	Bulk	374.5 ± 0.2	19.7 ± 3.6	61 ± 13	105 ± 3	122 ± 4
	71	369.0 ± 0.3	10.4 ± 1.2	32 ± 6	102 ± 7	120 ± 9
	47	365.2 ± 0.5	9.0 ± 1.2	29 ± 7	95 ± 10	113 ± 12
	20	362.3 ± 0.3	10.6 ± 0.8	45 ± 5	70 ± 3	84 ± 4

^aGlass transition value at a reference cooling of 0.1 K/s.

We note that the apparent activation energy for glass formation E_a/R and the dynamic fragility m are measures of the temperature dependence of the relaxation time (or conversely, measures of the cooling rate dependence of T_g) and the slope of $\log \tau$ vs T (or T_g vs $\log q$) obviously depends on the reference temperature or reference T_{go} , taken here to be the value at a cooling rate of 0.1 K/s.

For the 350 nm-diameter rods, we obtain a normalized activation energy of 113 ± 9 kK and a fragility of 131 ± 11, very similar to the bulk values of $E_a = 105 \pm 4$ kK and $m = 122 \pm 4$ obtained earlier in our laboratory² using Flash DSC over a similar range of cooling rates. These values are considerably smaller than those that we and others have obtained from conventional DSC: For polystyrenes having molecular weight above ~30 000 g/mol (which has been shown in the work of Robertson et al. 72 to be the molecular weight above which the fragility of polystyrene is independent of molecular weight), the value of m has been reported to range from As the works of both Dhotel and co-workers⁷⁸ and Arellano and McKenna⁷⁹ have pointed out, however, the range of cooling rates used to obtain the fragility is important. Typically, that range is limited to one or two decades using conventional DSC, with the majority of the rates being slower than the typical reference rate of 10 K/min; since the temperature dependence of the relaxation time becomes stronger at low temperatures, this results in an overestimation of the fragility. On the other hand, Flash DSC can access many decades of cooling rates (e.g., from 0.1 to 3000 K/s used in this work), but the majority of these rates are higher than 10 K/min and this can result in an underestimation of the fragility if the range is not broad enough to get a good WLF fit. Interestingly, the work of Dhotel et al. 78 showed that combining conventional and Flash DSC data gave fragility values that were in agreement with those obtained from broadband spectroscopy, implying that this approach gives a more accurate value. We similarly used both conventional and Flash DSC for our bulk data, as shown in Fig. 4, yielding a fragility of 122 ± 4.2

The normalized activation energy E_a decreases with decreasing nanorod diameter from a value of 113 kK for 350 nm-diameter unsupported rods, similar to the bulk value of 105 and to 62 kK for 20 nm-diameter unsupported rods, comparable to the value for

20 nm supported ultrathin films. 1,2,21 The dynamic fragilities (m) follow the same trend, decreasing with decreasing diameter, from 131 to 76 for 350 and 20 nm rods, respectively. The 20 and 55 nm unsupported PS rods have a reduced fragility compared with the bulk and also compared with the thickest thin films (71 and 47 nm-thick), but their fragility is the same as that of the 20 nm ultrathin film within the error of measurements. However, in spite of the similarities of activation energy and dynamic fragility, the T_g depression of the 20 nm-diameter unsupported polystyrene nanorods is 8 K larger at a cooling rate of 0.1 K/s than that of a supported 20 nm ultrathin film.

The heat flow curves and depressed glass transition temperature of the 20 nm unsupported PS nanorods are stable with respect to the Flash DSC thermal history, which involves multiple scans with an isothermal hold at 180 °C for 6 s after each heating scan. This is presumably due to the relatively long time for interpenetration of chains from neighboring nanorods. For example, the estimated time for the molecules to diffuse one radius of gyration ($R_g = 30 \text{ nm}^{80}$) based on the self-diffusion coefficient (0.8 \times 10⁻¹⁵ cm²/s) at 170 $^{\circ}$ C for polystyrene of $M_w = 1000 \text{ kg/mol}$ is $\sim 2 \text{ h.}^{20,81}$ In order to further prove that the Tg depression observed is not an artifact caused by degradation of the material, we perform a combination of compression and thermal annealing under an inert environment at 170 °C for 5 h in a platen press at 10, 000 psi, which results in reversion of the rods to bulk behavior, as shown in Fig. 5. We note that simple annealing (without compression) at 170 °C for 5 h did not result in reversion of the film; this was similar to our observation for stacked thin films (which required pressure to revert to bulk),²⁰ but differed from single thin films, which dewet and thickened (and thereby, reverted to the bulk) under simple thermal treatment.¹

In order to test the importance of the free surface, we plot the magnitude of the T_g depression as a function of characteristic length scale ($h^* = V/S$, where V is the volume and S is the surface area) in Fig. 6 for our unsupported nanorods compared with data on polystyrene ultrathin films, 1,2,5,10 stacked thin films, 21 nanowires from the work of Zhu and co-workers, 39 and nanospheres from Priestley and co-workers 43 and from Cangialosi and co-workers. The characteristic length is taken to be as follows:

^bFrom Ref. 2

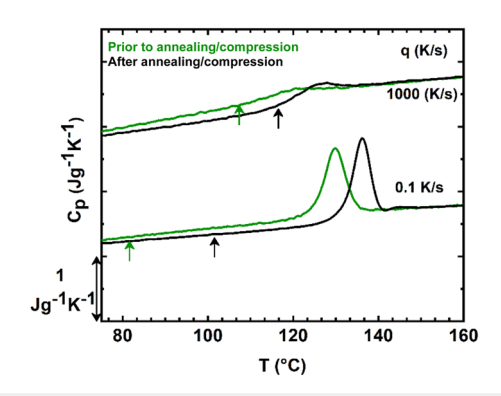


FIG. 5. Comparison of heat flow scans of 20 nm unsupported PS rods before and after annealing/compression treatment for 5 h at $170\,^{\circ}$ C in the platen press at $10\,000$ psi.

- h* = film thickness (h) for supported ultrathin films in direct contact with a hard substrate (e.g., those directly spin-coated onto silica).
- h* = h/2 for stacked ultrathin films or films with a soft interface between the film and substrate.
- $h^* = d/4$ for 2D nanorods and nanowires of diameter d.
- $h^* = d/6$ for 3D nanospheres.

The T_g depressions observed for our nanorods agree very well with our single thin film data and stacked thin film data when plotted vs the characteristic length scale, with all of the data lying between Roth and Dutcher's limits (dashed lines)⁵ and near Keddie

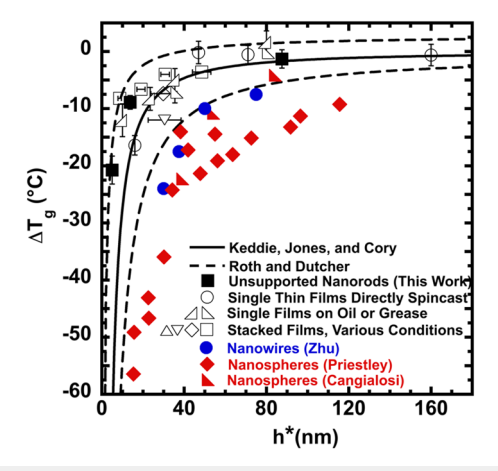


FIG. 6. Magnitude of T_g depressions (ΔT_g) at 0.1 K/s for unsupported PS nanorods (filled black squares) and single ultrathin PS films directly spincast (open circles), on oil (open right triangles), and on apiezon grease (open left triangles); stacked thin films from conventional DSC²¹ with ΔT_g obtained at 10 K/min, initially wrinkled (open squares), with PIB interleaving (open diamonds), initially flat by spin-coating onto Teflon from cosolvent (inverted triangles) and from toluene (open triangles). Also shown are data from the literature: PS nanowires in aqueous dispersion (filled blue circles) from the work of Zhu and co-workers; PS nanospheres in aqueous dispersion (filled red diamonds) from Priestley and co-workers; and PS nanospheres on PDMS from Cangialosi and co-workers (filled red left triangle). The black dashed lines are Roth and Dutcher's upper and lower limits, and the solid black line is obtained from the work of Keddie *et al.* 9,10

and Jones' Eq. (1) (solid line), 10 noting that we assumed $h^* = h$ for both results from Keddie and Jones and from Roth and Dutcher's since these fits were obtained for thin films on hard substrates (i.e., having one mobile free surface). For our stacked thin films, on the other hand, we have assumed $h^* = h/2$ because the surfaces of the films do not interpenetrate during the time scale of the experiments due to the high molecular weight used; we used a similar assumption for the unsupported rods (with $h^* = d/4$), assuming that although they may touch one another, their surfaces are distinct and chains are confined to an individual rod during the time scale of the measurements. On the other hand, the $\Delta T_g s$ values of 2D polystyrene nanowires in aqueous dispersion from Zhu and co-workers³⁹ show a stronger T_g depression and sit just below the lower limit of Roth and Dutcher's compiled data set from the literature. Whether the differences between Zhu's nanowires dispersed in water and our nanorods having ionic liquid as a thermal conduction medium (that latter of which gives only a 2 K difference in Tg relative to rods without ionic liquid) are attributable to the difference in sample environment and/or method of preparation (Zhu's nanowires were prepared by electrospinning) or some other factor is unclear. However, Priestley's nanospheres in an aqueous dispersion⁴³ also show large Tg depressions, near or below Roth and Dutcher's lower limit, in good agreement with Zhu's nanowires and consistent with Cangiolosi's nanospheres, where the latter were dried and characterized by Flash DSC on polydimethylsiloxane (PDMS).⁴⁵ Hence, even though a simple free surface to volume argument may explain the relationship between our thin film and nanorod data, this scaling does not fully explain the effect of nanoconfinement on Tg (as shown by the data in Fig. 4). This result is perhaps not surprising in light of the work showing the influence of substrate and interfaces on Tg changes. 9,12,15–17,26,27,29,31,32,35–39,42,43

Enthalpy recovery

Enthalpy recovery was studied for the 20 and 350 nm-diameter unsupported nanorods at temperatures ranging from 4 K above to 87 K below the limiting fictive temperature at 1000 K/s. Representative data are plotted as the departure from equilibrium, $T_f - T_a$, vs logarithm aging time in Fig. 7(a) for the enthalpy recovery of 20 and 350 nm-diameter nanorods, respectively; also shown are data for bulk polystyrene and for 20 nm polystyrene ultrathin films from previous work. ^{2,46–49} Since the T_{fo} values of the four samples shown differ, the enthalpy recovery comparison is made at similar jump sizes $(T_{fo} - T_a)$ rather than similar aging temperatures; hence, the initial values are similar for all the samples. The time at which $T_{fo} - T_a$ starts to evolve toward zero (where $T_f = T_a$) has been termed the induction time (t_{ind}), and this time scale is considered to be a measure of the shortest effective segmental relaxation time. Interestingly, the induction times are similar for all four samples, with a temperature dependence of ~20 K/decade.

After the induction period, the departure from equilibrium $(T_{fo}-T_a)$ decreases linearly with logarithm of aging time. Structural recovery is monotonic, which is in contrast to intermediate plateaus reported by Perez-De-Eulate and Cangialosi for polystyrene nanospheres at time scales as small as 100 s for 230 nm nanospheres aged at 353 K $(T_{fo}-T_a=31 \text{ K})$. The time scale to reach equilibrium, which is a measure of the longest effective segmental relaxation time, increases logarithmically with decreasing

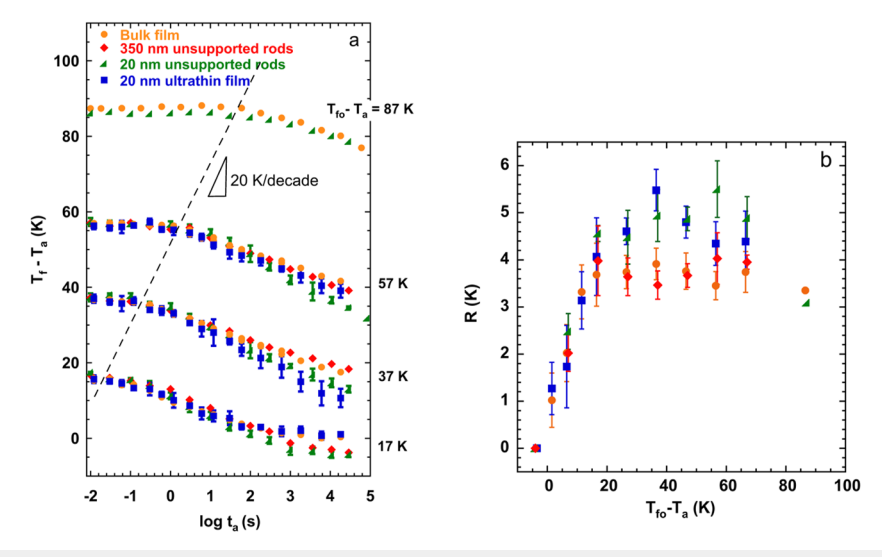


FIG. 7. (a) Representative change in fictive temperature relative to T_a during enthalpy recovery vs log t_a for different jump sizes from T_{fo} for 20 nm-diameter (green triangles) and 350 nm-diameter (red diamonds) unsupported polystyrene nanorods, as compared with previous data for 20 nm ultrathin PS film (blue squares) and bulk (orange circles) from previous work. 2.44-47 (b) Aging rate as a function of jump size ($T_{fo} - T_a$).

temperature, and hence, these time scales are obtained only for the highest aging temperatures studied. The rate of aging (R, in K/decade) can be obtained from the slope of linear region of T_f - T_a vs logarithm aging time:

$$R = \frac{-d(T_f - T_a)}{d\log t_a}. (7)$$

Rates are compared in Fig. 7(b) for the 20 and 350 nm unsupported nanorods, the 20 nm ultrathin film and the bulk as a function of jump sizes. Consistent with Struik's early work, 83 the aging rate goes to zero for $T_a > T_{fo}$, increases with decreasing aging temperature, and goes through a maximum some 40–60 K below T_{fo} . The aging rates of the bulk and 350 nm unsupported rods are very similar

at all jump sizes, whereas those of the 20 nm unsupported rods and 20 nm ultrathin film are slightly higher than bulk for jump sizes from 20 to 60 K below T_{fo} . Within the error of measurement, the 20 nm unsupported rods and 20 nm ultrathin film have similar aging rates when compared at a given jump size (or same distance from T_g).

DISCUSSION

The time scales associated with both the cooling rate dependence of T_g and the enthalpy recovery process are plotted on a relaxation map for the unsupported 20 and 350 nm-diameter nanorods and compared with results for 20 nm ultrathin films and bulk polystyrene, as shown in Fig. 8, where the x-axis is taken as temperature in Fig. 8(a) and as the temperature departure from

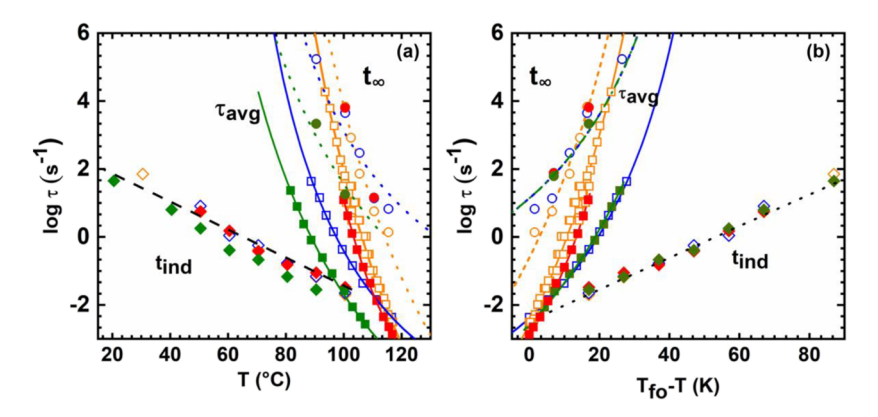


FIG. 8. Relaxation time map including induction times (t_{ind} ; diamonds), average relaxation times (squares), and times to reach equilibrium (t_{∞} , circles) as a function of (a) T_{ind} and (b) $T_{ind} - T_{ind}$ are shown for 20 (solid green symbols) and 350 nm (solid red symbols) supported nanorods along with 20 nm ultrathin PS film^{2,46} (open blue symbols) and bulk^{1,21,47,48} (open orange symbols). The black dashed line is linear fit to all the induction times. The colored solid lines (red, blue and green) are the WLF dependence of average relaxation times obtained using the cooling rate dependence of T_g . The colored short-dashed lines are the same WLF dependence data shifted by a constant to fit the data for the time scale required to reach equilibrium.

the reference T_{fo} obtained at 1000 K/s in Fig. 8(b). The average relaxation time (τ_{avg}) from the T_g studies is based on the relationship developed by Hodge⁸⁴ using the Deborah number (DN), which can be expressed in terms of the rate of change of effective time scale during cooling $(d\tau/dt)$, leading to the following relationship between the average relaxation time and the cooling rate q: $\tau_{ave} = RT_g^2/E_aq$, where E_a/R is the normalized activation energy reported in Table I. In addition, the induction time (t_{ind}) and the time required to reach equilibrium (t_{∞}) as a function of aging temperature from the enthalpy recovery studies are plotted. The former values are determined from data such as those shown in Fig. 7 from the intersection of the initial plateau in $T_f - T_a$ with the linear fit obtained from the data up to 3 decades after the initial drop in $T_f - T_a$. On the other hand, the time required to reach equilibrium is obtained from the T_f - T_a data close to equilibrium using the following equation:

$$t_{\infty} = \tau_0 \left[\ln \left(\frac{T_{fo} - T_a}{T_{f\infty} - T_a} \right) \right]^{1/\beta}, \tag{8}$$

where relaxation time τ_0 and nonexponentiality parameter β are the KWW parameters, $T_{fo}-T_a$ is the initial departure from equilibrium temperature, and the time to reach equilibrium is defined as the time taken to reach $T_{f\infty}-T_a=0.035$ K, as reported in other work. ⁵¹

The average relaxation times follow the same WLF temperature dependence as that of T_f vs log q. Hence, the 350 nm unsupported nanorods behave very similarly to the bulk. Interestingly, the average relaxation times of 20 nm unsupported PS rods and 20 nm ultrathin PS film have similar temperature dependence when compared as a function $T_{fo}-T$, in spite of the difference of 8 K in their T_g (or T_{fo}) values. The similarity in the temperature dependence of the average relaxation times of 20 nm unsupported rods and 20 nm ultrathin film may also be the reason for similar enthalpy recovery behavior irrespective of the difference in magnitude of T_g depression and spatial dimensionality.

All of the materials have the same induction times in the glassy state when compared as a function of $T_{fo}-T_a$. The implication is that the shortest effective segmental relaxation times are not significantly perturbed by nanoscale confinement. On the other hand, the times required to reach equilibrium for the 20 nm unsupported rods and the 20 nm thin films have a different and much weaker temperature dependence compared with that of the bulk and the 350 nm unsupported rods. The implication is that although the time scales to reach equilibrium are similar for high aging temperature near T_{fo} , they diverge at lower temperatures, with the 20 nm rods and thin films reaching equilibrium faster than the bulk or 350 nm rods

The relaxation map also tells us something about the respective breadths of the segmental relaxation times for nanoconfined and bulk samples. The difference between the average relaxation time and the longest relaxation at a given temperature departure from T_{fo} is the same for the 20 nm-diameter rod and the 20 nm-thick ultrathin film, in spite of the difference in their T_g s, and is much larger than for the 350 nm-diameter rod and the bulk sample, consistent with many previous studies that found that nanoconfinement increases the distribution of relaxation times. Furthermore, the relaxation time map explains much of the discrepancy in the literature for the T_g depression—different results will be obtained

depending not only on the time scale of the measurement but also on how the experimental measurement weights the relaxation times in the system.

CONCLUSIONS

The glass transition behavior of AAO supported and unsupported polystyrene nanorods was studied using the Flash DSC at cooling rates spanning four decades. The glass transition temperatures were found to be similar to the bulk for supported nanorods in AAO and for those having a diameter of 350 nm. On the other hand, 20 and 55 nm unsupported nanorods were found to depressed by 20.1 \pm 2.2 and 8.8 \pm 0.7 K when compared to the bulk, respectively, at a cooling rate of 0.1 K/s. In addition, a Tg depression of 9.4 ± 1.6 was also observed at 1000 K/s for the 20 nm-diameter nanorod, in contrast with the 20 nm ultrathin films where no T_g depression was observed at high rates.² An effect of spatial dimensionality on the T_g depression was observed, with the magnitude of T_g depression for 20 nm unsupported PS rods being 8 K higher than that of the 20 nm ultrathin PS film (at 0.1 K/s). Interestingly, the T_g depressions for the nanorods and ultrathin films were consistent when plotted as a function of the characteristic length scale (volume/surface area) and fell within the literature data compiled by Roth and Dutcher.⁵ However, the larger depressions for nanowires and nanospheres in the literature suggest that the effect of spatial dimensionality is more complex than a simple volume to surface scaling. The enthalpy recovery process of the 20 and 350 nm unsupported nanorods was also investigated and found to be linear and monotonic for all jump sizes. The induction times for both 20 and 350 nm unsupported nanorods were similar and also in good agreement with the induction times of 20 nm ultrathin film and bulk data from previous studies in our laboratory when compared at similar distances from Tfo. The overall enthalpy recovery rate of 20 nm unsupported nanorods was found to be similar to that of 20 nm ultrathin film and faster than that of the bulk and 350 nm nanorods. In addition, the fragilities and the relaxation maps of the 20 nm nanorods and 20 nm ultrathin films were similar in spite of the 8 K difference in their T_g values.

ACKNOWLEDGMENTS

The authors gratefully acknowledge the funding from Grant No. NSF DMR 1610614, as well as Grant No. NSF DMR 2141221. The authors would like to thank Dr. Kristin M. Hutchins from the Department of Chemistry and Biochemistry at Texas Tech University for use of the GPC for molecular weight measurements. The authors would also like to thank Dr. Heedong Yoon for measuring the thicknesses of polystyrene films.

AUTHOR DECLARATIONS

Conflict of Interest

The authors have no conflicts to disclose.

Author Contributions

Madhusudhan R. Pallaka: Data curation (equal); Formal analysis (equal). **Sindee L. Simon**: Conceptualization (lead); Funding acquisition (lead).

DATA AVAILABILITY

The data that support the findings of this study are available from the corresponding author upon reasonable request.

REFERENCES

- Y. Gao, Y. P. Koh, and S. L. Simon, "Calorimetric glass transition of single polystyrene ultrathin films," Macromolecules 46(2), 562–570 (2013).
 Y. P. Koh and S. L. Simon, "The glass transition and enthalpy recovery of a
- ²Y. P. Koh and S. L. Simon, "The glass transition and enthalpy recovery of a single polystyrene ultrathin film using Flash DSC," J. Chem. Phys. **146**(20), 203329 (2017).
- ³ M. Alcoutlabi and G. B. McKenna, "Effects of confinement on material behaviour at the nanometre size scale," J. Phys.: Condens. Matter **17**(15), R461 (2005).
- ⁴G. B. McKenna and S. L. Simon, "50th Anniversary Perspective: Challenges in the dynamics and kinetics of glass-forming polymers," Macromolecules **50**(17), 6333–6361 (2017).
- ⁵C. B. Roth and J. R. Dutcher, "Glass transition and chain mobility in thin polymer films," J. Electroanal. Chem. **584**(1), 13–22 (2005).
- ⁶S. Napolitano, E. Glynos, and N. B. Tito, "Glass transition of polymers in bulk, confined geometries, and near interfaces," Rep. Prog. Phys. **80**(3), 036602 (2017).
- ⁷M. Ediger and J. Forrest, "Dynamics near free surfaces and the glass transition in thin polymer films: A view to the future," Macromolecules 47(2), 471–478 (2013).
- ⁸R. Richert, "Dynamics of nanoconfined supercooled liquids," Annu. Rev. Phys. Chem. **62**, 65–84 (2011).
- ⁹J. L. Keddie, R. A. Jones, and R. A. Cory, "Interface and surface effects on the glass-transition temperature in thin polymer films," Faraday Discuss. **98**, 219–230 (1994).
- ¹⁰J. Keddie and R. Jones, "Glass transition behavior in ultra-thin polystyrene films," Isr. J. Chem. 35(1), 21–26 (1995).
- ¹¹ J. A. Forrest and K. Dalnoki-Veress, "The glass transition in thin polymer films," Adv. Colloid Interface Sci. 94(1-3), 167–195 (2001).
- ¹²J. Forrest, K. Dalnoki-Veress, and J. Dutcher, "Interface and chain confinement effects on the glass transition temperature of thin polymer films," Phys. Rev. E 56(5), 5705 (1997).
- ¹³Z. Fakhraai and J. A. Forrest, "Probing slow dynamics in supported thin polymer films," Phys. Rev. Lett. 95, 025701 (2005).
- ¹⁴C. J. Ellison and J. M. Torkelson, "The distribution of glass-transition temperatures in nanoscopically confined glass formers," Nat. Mater. 2, 695–700 (2003).
- ¹⁵C. B. Roth and J. M. Torkelson, "Selectively probing the glass transition temperature in multilayer polymer films: Equivalence of block copolymers and multilayer films of different homopolymers," Macromolecules **40**(9), 3328–3336 (2007).
- 16 C. M. Evans, S. Y. Kim, C. B. Roth, R. D. Priestley, L. J. Broadbelt, and J. M. Torkelson, "Role of neighboring domains in determining the magnitude and direction of $T_{\rm g}$ -confinement effects in binary, immiscible polymer systems," Polymer 80, 180–187 (2015).
- ¹⁷C. B. Roth, K. L. McNerny, W. F. Jager, and J. M. Torkelson, "Eliminating the enhanced mobility at the free surface of polystyrene: Fluorescence studies of the glass transition temperature in thin bilayer films of immiscible polymers," Macromolecules 40(7), 2568–2574 (2007).
- ¹⁸ J. E. Pye and C. B. Roth, "Above, below, and in-between the two glass transitions of ultrathin free-standing polystyrene films: Thermal expansion coefficient and physical aging," J. Polym. Sci., Part B: Polym. Phys. 53(1), 64–75 (2015).
 ¹⁹ J. E. Pye and C. B. Roth, "Two simultaneous mechanisms causing glass transitions."
- ¹⁹J. E. Pye and C. B. Roth, "Two simultaneous mechanisms causing glass transition temperature reductions in high molecular weight freestanding polymer films as measured by transmission ellipsometry," Phys. Rev. Lett. **107**(23), 235701 (2011).
- ²⁰Y. P. Koh, G. B. McKenna, and S. L. Simon, "Calorimetric glass transition temperature and absolute heat capacity of polystyrene ultrathin films," J. Polym. Sci., Part B: Polym. Phys. 44(24), 3518–3527 (2006).
- ²¹Y. P. Koh and S. L. Simon, "Structural relaxation of stacked ultrathin polystyrene films," J. Polym. Sci., Part B. Polym. Phys. **46**(24), 2741–2753 (2008).

- ²²H. Yin, D. Cangialosi, and A. Schönhals, "Glass transition and segmental dynamics in thin supported polystyrene films: The role of molecular weight and annealing," Thermochim. Acta **566**, 186–192 (2013).
- 23 V. M. Boucher, D. Cangialosi, H. Yin, A. Schönhals, A. Alegría, and J. Colmenero, " T_g depression and invariant segmental dynamics in polystyrene thin films," Soft Matter **8**(19), 5119–5122 (2012).
- ²⁴M. Tress, M. Erber, E. U. Mapesa, H. Huth, J. Muller, A. Serghei, C. Schick, K.-J. Eichhorn, B. Voit, and F. Kremer, "Glassy dynamics and glass transition in nanometric thin layers of polystyrene," <u>Macromolecules</u> 43(23), 9937–9944 (2010).
- ²⁵P. A. O'Connell, S. A. Hutcheson, and G. B. McKenna, "Creep behavior of ultra-thin polymer films," J. Polym. Sci., Part B: Polym. Phys. **46**(18), 1952–1965 (2008).
- ²⁶H. Yoon and G. B. McKenna, "Substrate effects on glass transition and free surface viscoelasticity of ultrathin polystyrene films," Macromolecules 47(24), 8808–8818 (2014).
- ²⁷J. Wang and G. B. McKenna, "Viscoelastic and glass transition properties of ultrathin polystyrene films by dewetting from liquid glycerol," Macromolecules 46(6), 2485–2495 (2013).
- ²⁸Z. Yang, Y. Fujii, F. K. Lee, C.-H. Lam, and O. K. Tsui, "Glass transition dynamics and surface layer mobility in unentangled polystyrene films," Science 328(5986), 1676–1679 (2010).
- ²⁹G. DeMaggio, W. Frieze, D. Gidley, M. Zhu, H. Hristov, and A. Yee, "Interface and surface effects on the glass transition in thin polystyrene films," Phys. Rev. Lett. 78(8), 1524 (1997).
- ³⁰ K. Fukao and Y. Miyamoto, "Glass transitions and dynamics in thin polymer films: Dielectric relaxation of thin films of polystyrene," Phys. Rev. E **61**(2), 1743 (2000).
- ³¹ A. V. Lyulin, N. K. Balabaev, A. R. Baljon, G. Mendoza, C. W. Frank, and D. Y. Yoon, "Interfacial and topological effects on the glass transition in free-standing polystyrene films," J. Chem. Phys. 146(20), 203314 (2017).
- ³²D. S. Fryer, R. D. Peters, E. J. Kim, J. E. Tomaszewski, J. J. de Pablo, P. F. Nealey, C. C. White, and W. L. Wu, "Dependence of the glass transition temperature of polymer films on interfacial energy and thickness," Macromolecules 34(16), 5627–5634 (2001).
- ³³G. Kim and M. Libera, "Morphological development in solvent-cast Polystyrene–Polybutadiene–Polystyrene (SBS) triblock copolymer thin films," <u>Macromolecules</u> 31(8), 2569–2577 (1998).
- ³⁴N. Shamim, Y. P. Koh, S. L. Simon, and G. B. McKenna, "Glass transition temperature of thin polycarbonate films measured by flash differential scanning calorimetry," J. Polym. Sci., Part B: Polym. Phys. **52**(22), 1462–1468 (2014).
- ³⁵E. S. Kang, B. Graczykowski, U. Jonas, D. Christie, L. A. G. Gray, D. Cangialosi, R. D. Priestley, and G. Fytas, "Shell architecture strongly influences the glass transition, surface mobility, and elasticity of polymer core-shell nanoparticles," Macromolecules 52, 5399–5406 (2019).
- ³⁶R. Katsumata, A. R. Dulaney, C. B. Kim, and C. J. Ellison, "Glass transition and self-diffusion of unentangled polymer melts nanoconfined by different interfaces," Macromolecules **51**, 7509–7517 (2018).
- ³⁷ H. J. Kim, Y. Cang, E. Kang, B. Graczykowski, M. Secchi, M. Montagna, R. D. Priestley, E. M. Furst, and G. Fytas, "Direct observation of polymer surface mobility via nanoparticle vibrations," Nat. Commun. 9, 2918 (2018).
- ³⁸S. Liu, M. Q. Lv, H. R. Li, S. Wang, C. D. Feng, X. L. Wang, W. B. Hu, and W. Wang, "Optical imaging of the molecular mobility of single polystyrene nanospheres," J. Am. Chem. Soc. **144**, 1267–1273 (2022).
- ³⁹W. Wei, S. Feng, Q. Zhou, H. Liang, Y. Long, Q. Wu, H. Gao, G. Liang, and F. Zhu, "Study on glass transition and physical aging of polystyrene nanowires by differential scanning calorimetry," J. Polym. Res. **24**(3), 38 (2017).
- ⁴⁰S. Askar, T. Wei, A. W. Tan, and J. M. Torkelson, "Molecular weight dependence of the intrinsic size effect on T_g in AAO template-supported polymer nanorods: A DSC study," J. Chem. Phys. 146(20), 203323 (2017).
- ⁴¹S. Alexandris, P. Papadopoulos, G. Sakellariou, M. Steinhart, H.-J. R. Butt, and G. Floudas, "Interfacial energy and glass temperature of polymers confined to nanoporous alumina," Macromolecules **49**(19), 7400–7414 (2016).
- ⁴²C. Teng, L. Li, Y. Wang, R. Wang, W. Chen, X. Wang, and G. Xue, "How thermal stress alters the confinement of polymers vitrificated in nanopores," J. Chem. Phys. **146**(20), 203319 (2017).

- ⁴³C. Zhang, Y. Guo, and R. D. Priestley, "Glass transition temperature of polymer nanoparticles under soft and hard confinement," Macromolecules 44(10), 4001-4006 (2011).
- ⁴⁴C. Zhang, V. M. Boucher, D. Cangialosi, and R. D. Priestley, "Mobility and glass transition temperature of polymer nanospheres," Polymer 54(1), 230-235
- ⁴⁵N. G. Perez-de-Eulate, V. Di Lisio, and D. Cangialosi, "Glass transition and molecular dynamics in polystyrene nanospheres by fast scanning calorimetry," ACS Macro Lett. 6, 859-863 (2017).
- ⁴⁶Y. P. Koh and S. L. Simon, "Enthalpy recovery of ultrathin polystyrene film using Flash DSC," Polymer 143, 40-45 (2018).
- 47 Y. P. Koh, S. Y. Gao, and S. L. Simon, "Structural recovery of a single polystyrene thin film using Flash DSC at low aging temperatures," Polymer 96, 182-187 (2016).
- ⁴⁸Y. P. Koh, L. Grassia, and S. L. Simon, "Structural recovery of a single polystyrene thin film using nanocalorimetry to extend the aging time and temperature range," Thermochim. Acta 603, 135-141 (2015).
- ⁴⁹L. Grassia, Y. P. Koh, M. Rosa, and S. L. Simon, "Complete set of enthalpy recovery data using flash DSC: Experiment and modeling," Macromolecules 51(4), 1549-1558 (2018).
- 50 E. Lopez and S. L. Simon, "Signatures of structural recovery in polystyrene by nanocalorimetry," Macromolecules 49, 2365-2374 (2016).
- ⁵¹ S. L. Simon, J. W. Sobieski, and D. J. Plazek, "Volume and enthalpy recovery of polystyrene," Polymer 42(6), 2555-2567 (2001).
- ⁵²Y. P. Koh and S. L. Simon, "Enthalpy recovery of polystyrene: Does a long-term aging plateau exist?," Macromolecules 46(14), 5815-5821 (2013).
- 53 V. M. Boucher, D. Cangialosi, A. Alegría, and J. Colmenero, "Enthalpy recovery in nanometer to micrometer thick polystyrene films," Macromolecules 45(12), 5296-5306 (2012).
- ⁵⁴J. E. Pye, K. A. Rohald, E. A. Baker, and C. B. Roth, "Physical aging in ultrathin polystyrene films: Evidence of a gradient in dynamics at the free surface and its connection to the glass transition temperature reductions," Macromolecules 43(19), 8296-8303 (2010).
- 55 P. F. Green, E. Glynos, and B. Frieberg, "Polymer films of nanoscale thickness: Linear chain and star-shaped macromolecular architectures," MRS Commun. 5(3), 423-434 (2015).
- 56 Y. Guo, C. Zhang, C. Lai, R. D. Priestley, M. D'Acunzi, and G. Fytas, "Structural relaxation of polymer nanospheres under soft and hard confinement: Isobaric versus isochoric conditions," ACS Nano 5(7), 5365-5373 (2011).
- 57 M. R. Pallaka, D. K. Unruh, and S. L. Simon, "Melting behavior of n-alkanes in anodic aluminum oxide (AAO) nanopores using Flash differential scanning calorimetry," Thermochim. Acta 663, 157-164 (2018).
- ⁵⁸J. M. G. Cowie, "Some general features of relations for oligomers and amorphous polymers," Eur. Polym. J. 11(4), 297-300 (1975).
- ⁵⁹ A. Toda and M. Konishi, "An evaluation of thermal lags of fast-scan microchip
- DSC with polymer film samples," Thermochim. Acta **589**, 262–269 (2014). ⁶⁰E. Zhuravlev and C. Schick, "Fast scanning power compensated differential scanning nano-calorimeter: 2. Heat capacity analysis," Thermochim. Acta 505(1-2), 14-21 (2010).
- $^{\bf 61}$ J. E. K. Schawe, "Measurement of the thermal glass transition of polystyrene in a cooling rate range of more than six decades," Thermochim. Acta 603, 128-134 (2015).
- 62 J. Martín, J. Maiz, J. Sacristan, and C. Mijangos, "Tailored polymerbased nanorods and nanotubes by "template synthesis": From preparation to applications," Polymer 53(6), 1149-1166 (2012).
- ⁶³M. Zhang, P. Dobriyal, J.-T. Chen, T. P. Russell, J. Olmo, and A. Merry, "Wetting transition in cylindrical alumina nanopores with polymer melts," Nano Lett. 6(5), 1075-1079 (2006).

- ⁶⁴A. Q. Tool, "Relation between inelastic deformability and thermal expansion of glass in its annealing range," J. Am. Ceram. Soc. 29(9), 240-253 (1946).
- ⁶⁵P. Badrinarayanan, W. Zheng, Q. Li, and S. L. Simon, "The glass transition temperature versus the fictive temperature," J. Non-Cryst. Solids 353(26), 2603–2612
- ⁶⁶C. T. Moynihan, A. J. Easteal, M. A. De Bolt, J. Tucker, and J. Tucker, "Dependence of the fictive temperature of glass on cooling rate," J. Am. Ceram. Soc. **59**(1-2), 12–16 (1976).
- 67 M. J. Richardson and N. G. Savill, "Derivation of accurate glass transition temperatures by differential scanning calorimetry," Polymer 16, 753-757
- ⁶⁸P. Cebe, B. P. Partlow, D. L. Kaplan, A. Wurm, E. Zhuravlev, and C. Schick, "Using flash DSC for determining the liquid state heat capacity of silk fibroin," Thermochim. Acta 615, 8-14 (2015).
- $^{\mathbf{69}}\mathrm{A.~A.~El}$ Banna and G. B. McKenna, "Challenging the Kauzmann paradox using an ultra-stable perfluoropolymer glass with a fictive temperature below the dynamic VFT temperature," Sci. Rep. 13, 4224 (2023).
- ⁷⁰H. D. Yoon, Y. P. Koh, S. L. Simon, and G. B. McKenna, "An ultrastable polymeric glass: Amorphous fluoropolymer with extreme fictive temperature reduction by vacuum pyrolysis," Macromolecules 50, 4562-4574 (2017).
- 71 M. L. Williams, R. F. Landel, and J. D. Ferry, "The temperature dependence of relaxation mechanisms in amorphous polymers and other glass-forming liquids," I. Am. Chem. Soc. 77(14), 3701–3707 (1955).
- 72 C. G. Robertson, P. G. Santangelo, and C. M. Roland, "Comparison of glass formation kinetics and segmental relaxation in polymers," J. Non-Cryst. Solids 275, 153-159 (2000).
- ⁷³C. Dalle-Ferrier, S. L. Simon, W. Zheng, P. Badrinarayanan, T. Fennell, B. Frick, J. M. Zanotti, and C. Alba-Simionesco, "Consequence of excess configurational entropy on fragility: The case of a polymer-oligomer blend," Phys. Rev. Lett. 103, 185702 (2009).
- ⁷⁴S. Askar, L. Q. Li, and J. M. Torkelson, "Polystyrene-grafted silica nanoparticles: Investigating the molecular weight dependence of glass transition and fragility behavior," Macromolecules 50, 1589-1598 (2017).
- $^{\bf 75}{\rm K.~L.}$ Jin and J. M. Torkelson, "Enhanced $t_{\rm g}\text{-confinement}$ effect in crosslinked polystyrene compared to its linear precursor: Roles of fragility and chain architecture," Macromolecules 49, 5092-5103 (2016).
- ⁷⁶T. Wang, A. Peera, J. Reffner, and J. M. Torkelson, "Reducing the bulk fragility and suppressing the fragility-confinement effect in polystyrene with very low levels of 2-ethylhexyl acrylate comonomer," Macromolecules 56, 3527-3537 (2023).
- 77 T. Sasaki, M. Ichimura, and S. Irie, "Correlation between fragility and cooperativity in segmental dynamics of glass-forming para-substituted polystyrenes," Polym. J. 47, 687-694 (2015).
- ⁷⁸ A. Dhotel, B. Rijal, L. Delbreilh, E. Dargent, and A. Saiter, "Combining flash DSC, DSC and broadband dielectric spectroscopy to determine fragility, J. Therm. Anal. Calorim. 121, 453-461 (2015).
- ⁷⁹A. K. Torres Arellano and G. B. McKenna, "Extremely fragile glass-formers? Calorimetric and rheological determinations," J. Polym. Sci., Part B: Polym. Phys. 53, 1261-1272 (2015).
- $^{\bf 80}$ M. Rubinstein and R. H. Colby, *Polymer Physics* (Oxford University Press, New York, 2003), Vol. 23.
- ⁸¹S. J. Whitlow and R. P. Wool, "Diffusion of polymers at interfaces: A secondary ion mass spectroscopy study," Macromolecules 24(22), 5926-5938 (1991).
- 82 N. G. Perez-De-Eulate and D. Cangialosi, "Double mechanism for structural recovery of polystyrene nanospheres," Macromolecules 51(9), 3299-3307 (2018). ⁸³L. C. E. Struik, Physical Aging in Amorphous Polymers and Other Materials
- (Elsevier Science, 1977). ⁸⁴I. M. Hodge, "Enthalpy relaxation and recovery in amorphous materials," J. Non-Cryst. Solids 169(3), 211-266 (1994).